ACS SyntheticBiology

Letter

pubs.acs.org/synthbio

Antigen Binding and Site-Directed Labeling of Biosilica-Immobilized Fusion Proteins Expressed in Diatoms

Nicole R. Ford,[†] Karen A. Hecht,[†] DeHong Hu,[‡] Galya Orr,[‡] Yijia Xiong,[§] Thomas C. Squier,[§] Gregory L. Rorrer,[∥] and Guritno Roesijadi*[,†,▽]

[†]Marine Biotechnology, Pacific Northwest National Laboratory, Sequim, Washington 98382, United States

[‡]Environmental Molecular Sciences Laboratory, Pacific Northwest National Laboratory, Richland, Washington 99352, United States

[§]Department of Basic Medical Sciences, Western University of Health Sciences, Lebanon, Oregon 97355, United States

[▽]Department of Microbiology, [∥]School of Chemical, Biological, and Environmental Engineering, Oregon State University, Corvallis, Oregon 97331, United States

Supporting Information

ABSTRACT: The diatom *Thalassiosira pseudonana* was genetically modified to express biosilica-targeted fusion proteins comprising either enhanced green fluorescent protein (EGFP) or single chain antibodies engineered with a tetracysteine tagging sequence. Of interest were the site-specific binding of (1) the fluorescent biarsenical probe AsCy3 and AsCy3e to the tetracysteine tagged fusion proteins and (2) high and low molecular mass antigens, the *Bacillus anthracis* surface layer protein EA1 or small molecule explosive trinitrotoluene (TNT), to biosilica-immobilized single chain antibodies. Analysis of biarsenical probe binding using fluorescence and structured illumination microscopy indicated differential colocalization with EGFP in nascent and mature biosilica, supporting the use of either EGFP or bound AsCy3 and AsCy3e in studying biosilica maturation. Large increases in the lifetime of a fluorescent analogue of TNT upon binding single chain antibodies provided a robust signal capable of discriminating binding to immobilized antibodies in the transformed frustule from nonspecific binding to the biosilica matrix. In conclusion, our results demonstrate an ability to engineer diatoms to create antibody-functionalized mesoporous silica able to selectively bind chemical and biological agents for the development of sensing platforms.

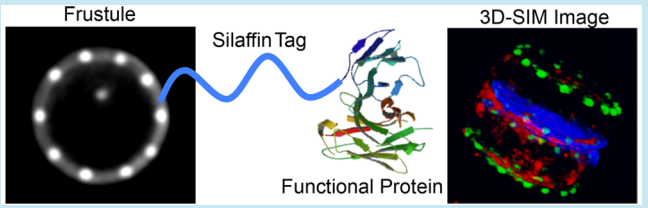

KEYWORDS: *diatom, silica, biarsenical probe, biosensor, TNT, anthrax*

Diatoms comprise a large, unicellular, microalgal taxon notable for constructing silica-based frustules[1] as their cell walls. The intricate patterning of diatom frustules has been the basis for constructing bioinspired hybrid protein-silica materials.[2] Genetic modification of diatoms to functionalize their mesoporous biosilica frustules with application-relevant proteins also has the potential to generate composite protein-silica functional materials[3] for applications in catalysis,[4] sensing,[5] and targeted drug delivery[6] and to better elucidate the biosilification process.[7,8]

In the diatom *Thalassiosira pseudonana*, silaffins and cingulins are trafficked to silica deposition vesicles (SDVs), where they participate in silica condensation and become part of the nascent frustule.[8,9] Consequently, fusing a protein with a desired function to either a silaffin or a cingulin results in trafficking of the chimeric protein to the frustule.[5,8,9]

The current repertoire of biosilica-immobilized functional proteins produced by genetic modification of diatoms and *in vivo* bioassembly does not include antibodies as binders for sensing and therapeutics or tetracysteine-tags for site-specific affinity labeling. To address these issues, we transformed *T. pseudonana* with silica-targeting expression vectors encoding single chain antibodies and tested their binding to large and small molecule antigens represented by the *B. anthracis* protein EA1 and the trinitrotoluene (TNT) surrogate trinitrobenzene (TNB). We also tested labeling of tetracysteine tagged proteins with biarsenical probes to assess the expression and localization of biosilica-targeted recombinant proteins.

Chimeric fusion genes encoded the silaffin tag $Sil3_{T8}$ for silica-targeting,[4,7] the tetracysteine Cy3TAG (CCKAEAACC)[10] for site-directed labeling with either the biarsenical probe AsCy3[10] or the cell-permeable methoxyester derivative AsCy3e,[11] and one of three functional proteins:

1. Enhanced green fluorescent protein (EGFP) to assess the efficacy of labeling live cells and isolated biosilica with the biarsenical probe AsCy3e and AsCy3, respectively, to establish a new tool for the study of diatom biosilica maturation.
2. A single domain antibody (sdAb) against the EA1 S-layer protein of *Bacillus anthracis* Sterne strain ($sdAb_{EA1}$)[12] to demonstrate functionality as a binder of a high molecular

Received: October 1, 2015
Published: January 8, 2016

DOI: 10.1021/acssynbio.5b00191
ACS Synth. Biol. 2016, 5, 193−199

weight protein antigen (a recombinant EA1-EGFP fusion protein).

3. A single chain variable fragment (scFv) against the explosive TNT ($scFv_{TNT}$)[13] to demonstrate functionality as a binder of a low molecular weight antigen (the fluorescent TNT surrogate, Alexa Fluor 555-TNB [AF555-TNB]).

We used Gateway (Invitrogen) technology to construct the diatom-specific expression clones $Sil3_{T8}$-Cy3TAG-EGFP for EGFP immobilization, $Sil3_{T8}$-Cy3TAG-$sdAb_{EA1}$ for $sdAb_{EA1}$ immobilization, and $Sil3_{T8}$-Cy3TAG-$scFv_{TNT}$ for $scFv_{TNT}$ immobilization (see Supplementary Methods for details of clone construction). *T. pseudonana* was transformed by biolistic bombardment using an established protocol.[14] Transformation with plasmid encoding only nourseothricin (NAT) resistance has a reported efficiency of about 420 transformants per 10^8 cells.[14] When paired with a plasmid encoding EGFP in a cotransformation, 80% of NAT-resistant clones expressed EGFP.[14] Instead of using the dual plasmid system originally described for this species, we adopted single-plasmid transformation (Figure S1) with separate transcription units for the selection factor and functional gene, each driven by the *T. pseudonana* constitutive *fcp* promoter.[4] Of the NAT-resistant clones that underwent secondary screening in our study, 50, 94, and 92% expressed the respective phenotypes for $Sil3_{T8}$-Cy3TAG-EGFP, $Sil3_{T8}$-Cy3TAG-$sdAb_{EA1}$, and $Sil3_{T8}$-Cy3TAG-$scFv_{TNT}$, similar to that described previously for cotransformation of *T. pseudonana*.[14] Of interest for future efforts is recently reported research to improve transformation of diatoms with episomal expression vectors delivered by bacterial conjugation.[15]

Using diatom cells expressing the $Sil3_{T8}$-Cy3TAG-EGFP fusion protein, we determined the colocalization[16] of AsCy3e, EGFP, and PDMPO (a fluorescent stain for newly forming diatom biosilica)[17] to assess binding of AsCy3e to the recombinant protein and association of the fusion protein with biosilica. Cells were synchronized,[18] then labeled with AsCy3e 4 h after synchrony release when the appearance of nascent biosilica would be apparent. Under these labeling conditions, the distribution of AsCy3e, EGFP, and PDMPO fluorescence coincided in the region of the nascent valves, signified by the emergence of additive colors in the images (Figure 1a,b). Our initial epifluorescence observations (Figure 1a) were confirmed by structured illumination microscopy (SIM) imaging (Figure 1b,c). SIM images were rendered in 3D using Volocity (Figure 1b), which optimizes fluorescent intensities, while single Z-stack frames were rendered using Zen (Figure 1c), which does not optimize fluorescence intensities. These two approaches to image analysis revealed different aspects of AsCy3e, EGFP, and PDMPO localization. AsCy3e was associated with both SDV- and nonSDV-associated structures. EGFP was localized to the valves, both mature and nascent, and was concentrated in the regions associated with rimoportulae. PDMPO, which targets newly forming biosilica,[17] was only associated with the nascent valve in the SDV.

Analyzing fluorescence intensity profiles for AsCy3e, EGFP, and PDMPO along a transect through the SDV (Figure 1c) indicated colocalization of AsCy3e labeling at positions enriched in EGFP within a broader background of PDMPO staining. The coincidence of AsCy3e, EGFP, and PDMPO in the SDV demonstrated that AsCy3e labeled the Cy3TAG-bearing recombinant protein during maturation of biosilica in

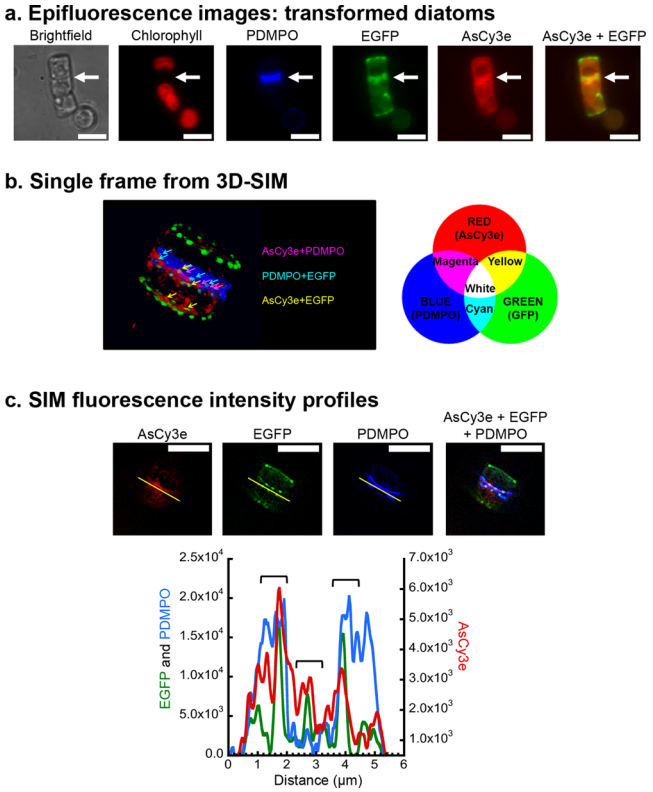

Figure 1. Colocalization of AsCy3e, PDMPO, and EGFP in transformed diatoms. Synchronized *T. pseudonana* cells expressing $Sil3_{T8}$-Cy3TAG-EGFP (green) were labeled with PDMPO (blue) and AsCy3e (red). (a) Epifluorescence imaging indicating PDMPO, EGFP, and AsCy3e at the SDV (arrows). (b) Single frame from a 3D-SIM movie (Figure S4) of a transformed diatom rendered in Volocity, showing colocalization of labels; color wheel shows colors associated with labels and their merges. (c) SIM images showing localization at the SDV and corresponding plot profile analysis along a transect (yellow) through the SDV (the regions of intersect with rimoportulae in the nascent valve are delineated by brackets in the graph). The fluorescence intensity profiles (arbitrary fluorescence units) indicated significant colocalization (Kendall's Coefficient of Concordance: W = 0.579, C^2 = 43.4217, 25 d.f., p = 0.0126) Scale bars = 5 μm.

the nascent valve. Weaker labeling with the AsCy3e probe could be seen in the mature valves at the periphery of the transect (Figure 1c).

Removal of organic material in the cell wall[19] during preparation of isolated frustules unmasked binding sites for exogenous small molecules. Thus, AsCy3 readily labeled the exposed biosilica of isolated frustules transformed with $Sil3_{T8}$-Cy3TAG-EGFP (Figure 2). SIM images showed that AsCy3 was colocalized with EGFP in the frustule, the nascent valve, and residual organic material entrapped within the frustule (Figure 2b). Fluorescence intensity profiles (Figure 2c) along the transect bisecting the AsCy3 and EGFP fluorescence images (Figure 2b) confirmed a highly significant colocalization of intensity peaks for AsCy3 and EGFP. The clusters of colocalized peaks in the plot profile aligned with mature and nascent valves and material entrapped within the frustule.

Overall, AsCy3-labeling of the $Sil3_{T8}$-Cy3TAG-EGFP fusion protein in isolated frustules was observed throughout the biosilica matrix (Figure 2). In contrast, site-directed AsCy3e labeling in live cells favored intracellular binding sites associated with nascent biosilica in the SDV and other subcellular

DOI: 10.1021/acssynbio.5b00191
ACS Synth. Biol. 2016, 5, 193−199

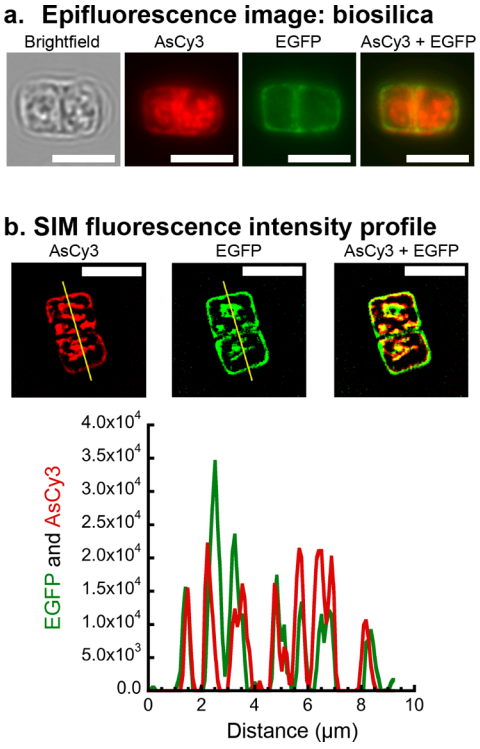

Figure 2. Colocalization of AsCy3 and EGFP in isolated biosilica from transformed diatoms. Biosilica was extracted from *T. pseudonana* cells expressing $Sil3_{T8}$-Cy3TAG-EGFP (green) and labeled with AsCy3 (red). (a) Epifluorescence imaging showing EGFP and AsCy3 colocalized throughout the entire frustule. (b) SIM images showing position of transects (yellow) bisecting the frustule. Fluorescence intensity profiles (arbitrary fluorescence units) indicated highly significant colocalization of AsCy3 and EGFP (Spearman's Rank Correlation: AsCy3 X EGFP, $r_s = -0.81$, 21 d.f., $p < 0.001$). Scale bars = 5 μm.

compartments, but not the mature frustule (Figure 1). Thus, the complex cell wall structure of live cells precluded ready interaction of the probe with the frustule, making isolated genetically modified frustules a more attractive platform for materials applications due to the increased accessibility of site-specific binding sites.

Having established the effectiveness of AsCy3 labeling of $Sil3_{T8}$-Cy3TAG-EGFP in isolated frustules (Figure 2), we applied it to labeling diatom frustules functionalized with single chain antibodies as binders for large and small molecule antigens, respectively represented by EA1 and TNT. *T. pseudonana* was transformed with expression clones containing fusion proteins $Sil3_{T8}$-Cy3TAG-$sdAb_{EA1}$ or $Sil3_{T8}$-Cy3TAG-$scFv_{TNT}$. While EGFP was suitable as a functional protein for following protein expression in diatoms expressing $Sil3_{T8}$-Cy3TAG-EGFP, EGFP was not a suitable reporter for expression of the single chain antibodies because the plasmids with fusion genes encoding a single chain antibody and a EGFP tag were linearized between the antibody and EGFP sequences during integration (Figure S2a,b), yielding only nonfluorescent NAT-resistant diatoms. Thus, EGFP was excluded from fusion genes encoding the single chain antibodies (Figures S2c,d and S3), and frustules were screened for protein expression using AsCy3 labeling (Figure 3). However, exclusion of EGFP as a tag for the sdAb permitted use of EA1-EGFP to assess antigen binding to the biosilica-immobilized $Sil3_{T8}$-Cy3TAG-$sdAb_{EA1}$.

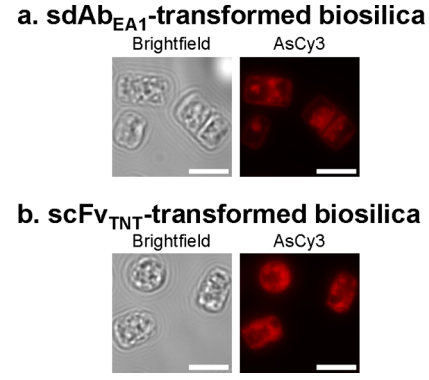

Figure 3. AsCy3 labeling of isolated diatom biosilica from single chain antibody-functionalized *T. pseudonana*. Epifluorescence images of biosilica extracted from *T. pseudonana* cells expressing (a) $Sil3_{T8}$-Cy3TAG- $sdAb_{EA1}$ or (b) $Sil3_{T8}$-Cy3TAG- $scFv_{TNT}$, and labeled with AsCy3 (red). Scale bars = 5 μm.

The ability of the biosilica-immobilized single chain antibodies to bind molecules differing in molecular mass by approximately two orders of magnitude was not impaired by the pore structure of the *T. pseudonana* biosilica. The respective target antigens, EA1-EFGP (121150 Da) and the TNT surrogate AF555-TNB (1243 Da), readily bound the transformed frustules (Figure 4). Binding of the larger EA1-GFP appeared to be restricted to the mature biosilica of transformed frustules (Figure 4a), whereas AF555-TNB also penetrated the biosilica and bound internal components in both native and transformed frustules (Figure 4b). The latter observation indicated a nonspecific component to interactions of AF555-

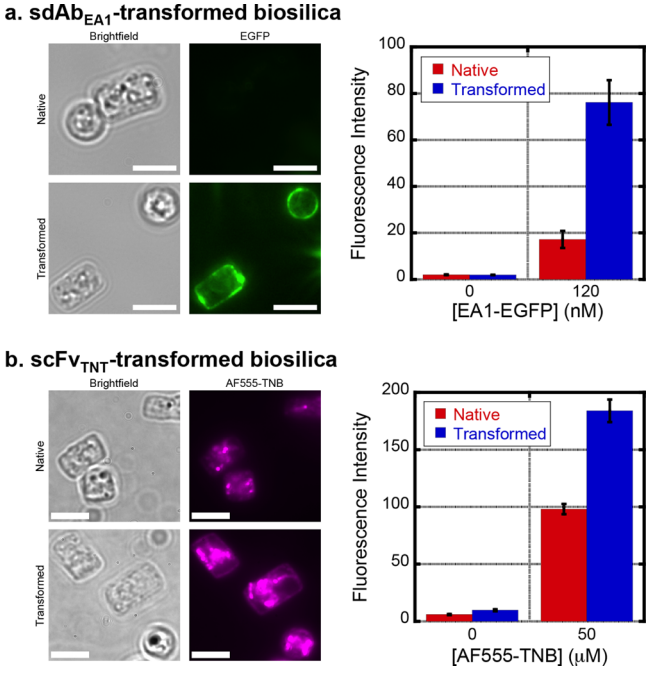

Figure 4. Fluorescent antigen binding to isolated diatom biosilica from single chain antibody-functionalized *T. pseudonana*. Epifluorescence images of extracted biosilica from transformed *T. pseudonana* cells. (a) EA1-EGFP fusion protein (green) bound to $Sil3_{T8}$-Cy3TAG-$sdAb_{EA1}$-functionalized biosilica. (b) AF555-TNB (magenta) bound to $Sil3_{T8}$-Cy3TAG-$scFv_{TNT}$-functionalized biosilica. Scale bars = 5 μm. Error bars represent 1 standard error.

DOI: 10.1021/acssynbio.5b00191
ACS Synth. Biol. 2016, 5, 193−199

TNB in native cells. These findings expanded the repertoire of recombinant proteins that can be genetically immobilized in diatom biosilica to include single chain antibodies for binding both large and small molecule antigens with topical relevance in environmental sensing and therapeutics.

We further analyzed the antigen−antibody complexation state as a function of the binding environment using frequency-domain fluorescence spectroscopy[20,21] to analyze isolated frustules, taking advantage of the environmental sensitivity of the Alexa Fluor dye in AF555-TNB.[22] Of specific interest was ascertaining the effect of silica immobilization of the $scFv_{TNT}$ on the fluorescence lifetime of the dye-labeled antigen. Mean lifetime values ($\bar{\tau}$) for the excited fluorophore complex (Table 1) were calculated from phase shift and modulation data (Figure S5).

Table 1. Mean Lifetime Measurements for AF555-TNB Bound to Free and Biosilica-Immobilized $scFv_{TNT}$[a]

experimental conditions	medium	scFV	mean lifetime, $\bar{\tau}$ (ns)
AF555-TNB	Solution	−	0.29
AF555-TNB + $scFv_{TNT}$	Solution	+	0.45
AF555-TNB + native frustules	Biosilica	−	1.45
AF555-TNB + $scFv_{TNT}$-transformed frustules	Biosilica	+	3.30

[a]See Figure S5 for graphs of phase shift, modulation, and their corresponding residuals.

Incremental increases in mean fluorescence lifetime occurred as the complexity of the binding environment increased (Table 1). The environmental sensitivity of AF555-TNB to both the biosilica medium and the presence or absence of $scFv_{TNT}$ suggested that the very large 10-fold increase in fluorescence lifetime upon association with the $scFv_{TNT}$-transformed frustules resulted from cumulative interactions with both the $scFv_{TNT}$-TNB binding site and the surrounding biosilica matrix.

We also noted that the presence of $scFv_{TNT}$, whether in solution or immobilized in biosilica, conferred similar relative increases in the mean fluorescence lifetime of approximately 2-fold above that observed in the absence of the $scFv_{TNT}$ (Table 1). This relative increase in fluorescence lifetime is consistent with the roughly 2-fold increase in fluorescence intensity of AF555-TNB binding to transformed frustules (Figure 4b). In addition, when the mean lifetime contributed by the biosilica matrix (represented by native frustules) was subtracted from that of the transformed frustules and compared to that resulting from binding the $scFv_{TNT}$ in solution, the resulting 4-fold increase in fluorescence lifetime over that of the $scFv_{TNT}$ in solution could be attributed to silica-immobilization of the $scFv_{TNT}$ [determined empirically from the following equation: Lifetime due to immobilized scFv/Lifetime of free scFv = $(\bar{\tau}_{\text{scFvTNT transformed frustule}} - \bar{\tau}_{\text{native frustule}})/\bar{\tau}_{\text{scFvTNT in solution}}$, assuming linearity of respective $\bar{\tau}$ values for native and transformed frustules].

The biosilica-immobilized proteins in the present study also retained function following isolation of frustules at 50 °C and rinsing with acetone (*e.g.*, Figures 2−4), indicating stability under potentially denaturing conditions. These observations are consistent with earlier reports that silica-immobilization of enzymes by genetic modification in diatoms confers added stability to enzyme activity when compared to enzymes in solution.[9]

We hypothesize that the increases in mean fluorescence lifetime and stability are due, in part, to oriented immobilization[23] of the recombinant protein in the diatom biosilica. The silaffin peptide tag would serve as both an anchor and a flexible tether that allows the appropriate protein motions needed for functional activities.

The present study extends the molecular toolbox for diatom cell biology and biotechnology to include labeling with biarsenical probes and functionalization of the biosilica frustule with single chain antibodies as binders for small and large molecule antigens. Labeling with biarsenical probes such as AsCy3 and AsCy3e will be useful for experiments intended to study the nature of the protein-silica environment and the interactions of proteins during the diatom biosilica maturation process. The cumulative interaction of the biosilica and scFv during antigen binding revealed by the fluorescence lifetime experiments indicated that the antigen−antibody binding surface and biosilica matrix are in close proximity, a potential problem if large antigens bind single chain antibodies that are immobilized within pores.[24] Therefore, the observation that EA1-GFP, with a Stokes radius of 5.1 nm,[25] readily bound to the transformed biosilica is quite remarkable and facilitates the design of antibody-based diatom biosensors in which antigen-availability is not restricted by the biosilica matrix.

In conclusion, the use of genetically modified diatom biosilica offers a robust approach to construction of functionalized mesoporous silica materials for sensing and other applications such as catalysis and therapeutics.

METHODS

Culture Conditions. Native and transformed cultures of *Thalassiosira pseudonana* (CCMP1335; Provasoli-Guillard National Center for Marine Algae and Microbiota) were maintained in artificial seawater (ESAW; https://ncma.bigelow.org/media/pdf/NCMAalgalmediumESAW.pdf) supplemented with 100 μg/mL penicillin (VWR) and 100 μg/mL streptomycin (Sigma-Aldrich) under continuous illumination on an orbital shaker (~10−40 μmol/m^2/sec, 20−22 °C) or in a Caron plant incubator (150 μmol/m^2/s, 20 °C) without agitation.

Expression Clone Construction. Multi-Site Gateway Pro cloning protocol was used to construct diatom-specific expression clones for biosilica targeted fusion proteins. Plasmids containing EGFP or the unmodified $scFv_{TNT}$[13] and $sdAb_{EA1}$ (clone A1)[12] sequences were used as templates for PCR. See Supplementary Methods for a full description of expression clone construction and integration.

Transformation of Diatoms. Diatoms were transformed by microparticle bombardment with a PDS-1000/He particle delivery system (Bio-Rad) using established procedures[14] with a 9 cm distance to the stopping screen and a 1550 psi rupture disk). Tungsten microcarrier (M-17/~0.7 μm diameter; Bio-Rad) was coated with 10 μg supercoiled plasmid DNA using the $CaCl_2$-spermidine method following manufacturer's instructions.

Isolation of Diatom Biosilica Frustules. Diatom frustules were isolated as previously described for detergent extraction at 50 °C with acetone rinse,[9] substituting 1% Igepal CA-630 (Sigma-Aldrich) for 1% SDS. For biosilica used in the fluorescence lifetime measurements, the isolation was conducted at 37 °C with agitation for 60 min, followed by three additional extractions with agitation for 5 min at 37 °C, three

DOI: 10.1021/acssynbio.5b00191
ACS Synth. Biol. 2016, 5, 193−199

water washes and one buffer wash (20 mM sodium phosphate pH 7.0, 100 mM EDTA).[9]

PDMPO and AsCy3e Labeling of Live Diatoms. Diatom cultures were synchronized by silicate deprivation and replenishment.[18] Following silicate starvation for 24 h, PDMPO (LysoSensor1 DND-160 yellow/blue, Life Technologies) was added to a final concentration of 1 μM and incubated for 5 min before addition of sodium silicate to a final concentration of 200 μM to release cells from starvation. Cells were harvested 4 h after synchronization and labeled with 0.5 μM AsCy3e in ESAW for 30 min at 25 °C in the dark. Labeled cells were washed twice in 5 mM dithiothreitol/PBS pH 7.4, twice in 2.5% (w/v) BSA/PBS pH 7.4, and twice in PBS pH 7.4. Cells were then fixed in 1% (v/v) paraformaldehyde/4% (w/v) sucrose/PBS pH 7.4 for 10 min at ambient temperature, then stored at 4 °C before imaging in 4% (w/v) sucrose/0.01% (w/v) sodium azide/PBS pH 7.4.

AsCy3 Labeling of Isolated Diatom Biosilica. Coverslips were coated with 0.1% branched polyethylenimine (PEI), MW ~ 2500 (Sigma-Aldrich) and dried overnight. Isolated diatom frustules were adhered to the PEI-coated coverslips overnight at 4 °C, protected from light. AsCy3 labeling of the frustules was performed on coverslips following the method of Hoffman *et al.* for FlAsH.[26] AsCy3-EDT_2 was used at a concentration of 0.5 μM (25 pmol per coverslip). Frustules were imaged under PBS.

Fluorescent Antigen Synthesis and Binding to Single Chain Antibodies. AF555-TNB was synthesized by conjugating TNB-sulfonic acid (Sigma-Aldrich) to AF555 cadaverine (Life Technologies) as previously described[27] and purified using Supelclean LC-18 SPE columns[27] or by C-18 reversed phase high performance liquid chromatography (RP-HPLC) with water/methanol gradients. Purity of the AF555-TNB was verified by analytical-scale C-18 RP-HPLC using AF555-TNB as a standard.

To construct the EA1-EGFP fusion protein, nucleotides 899914−902502 of the *B. anthracis eag* gene sequence (NCBI Reference Sequence NC_003997.3) were optimized for expression in *E. coli* and synthesized by Genewiz, Inc. MultiSite Gateway Pro (Invitrogen) cloning was used to construct the expression vector for EA1-EGFP (see Supporting Information). The expression clone pEXP2-EA1-EGFP was expressed in T7Express lysY/Iq *E. coli* cells (New England BioLabs). Cells were lysed by lysozyme digestion and sonication on ice in lysis buffer (20 mM sodium phosphate pH 8.0, 500 mM NaCl, 2 mM $MgCl_2$, 1 mM PMSF). Lysates were clarified by nuclease digestion (Pierce Universal Nuclease, Fisher) and centrifugation. The clarified supernatant was purified by Ni-affinity chromatography (Sepharose 6 Fast Flow resin, GE Healthcare), using manufacturer recommendations for purifying His-tagged proteins under native conditions. Imidazole was removed by buffer exchange in Amicon Ultra Centrifugal Filter Units (Millipore). Total protein concentration was calculated by BCA assay (Pierce). The fraction of EA1-EGFP in the enriched protein sample was estimated by quantification of the EA1-EGFP band from a Coomasie-stained gel using VisionWorksLS software (v.8.0 RC.1.2; UVP).

Isolated frustules transformed with either $Sil3_{T8}$-Cy3TAG-$scFv_{TNT}$ or $Sil3_{T8}$-Cy3TAG-$sdAb_{EA1}$ were incubated with fluorescently labeled antigen in PBS containing 0.05% Tween-20 (Fisher) and BSA Fraction V (Fisher) for 1 h at 4 °C followed by 1 h at room temperature (20−25 °C). The $scFv_{TNT}$ binding reaction used 0.05% BSA and 50 μM AF555-TNB; the $sdAb_{EA1}$ binding reaction used 1% BSA and 120 nM EA1-EGFP. Antigen-bound frustules were washed three times with PBS containing 0.05% Tween-20 prior to imaging in the same buffer on PEI-coated coverslips.

Epifluorescence Microscopy. Cells and isolated frustules were examined with a Leica DM IRB inverted epifluorescence microscope equipped with a mercury metal halide light source and liquid light guide (Leica). Four filter cubes were used to collect fluorescence with the following settings for Ex/DM/Em: (1) AsCy3/AsCy3e and AF555-TNB, 532−552/560/572−642 nm, (2) EGFP, 460−500/505/512−542 nm, (3) PDMPO, 382−392/409/468−552 nm, and (4) chlorophyll, 635−675/716/696−736 nm. Images were captured with a CoolSNAP Myo camera (Photometrics) and Metamorph software (v.7.7.11.0; Molecular Devices).

3D-SIM. SIM imaging was performed on a Zeiss Elyra S1 microscope using Plan-Apochromat 63× magnification (NA = 1.40) oil-immersion objective. Excitation of AsCy3/AsCy3e, EGFP, and PDMPO was achieved using 561, 488, and 405 nm laser excitation, respectively. Emission bandpass filters were 570−620 nm + LP 750 nm, 495−550 nm, and 495−550 nm, respectively. The excitation/emission color channels were recorded sequentially. Within each color channel, the raw data contained 3 rotations, 5 phases, and 0.110 μm spacing z stack images at 80 nm per pixel. Super-resolution images were reconstructed from raw images using Zeiss Efficient Navigation (ZEN) 2012 and Volocity 6.3.0 (PerkinElmer) software to generate 2D and 3D projections at 40 nm per pixel. Fluorescence intensity profiles for transects within a single optical section were constructed using the Plot Profile function in ImageJ 1.49v.[28]

Plot profiles for AsCy3e, EGFP, and PDMPO fluorescence intensities for the live cells were tested for the significance of colocalization using Kendall's Coefficient of Concordance.[29] For this analysis the entire data set of 138 points along each fluorescence transect was reduced to 25 degrees of freedom by sampling at every fifth point in order to reduce serial correlation arising from neighboring points. The significance of colocalization of AsCy3 and EGFP intensities in the 3D-SIM data for isolated frustules was tested using Spearman's Rank Correlation.[29] The data sets of 230 points for each fluorescence transect were reduced to 21 degrees of freedom by sampling every tenth point for the statistical analysis. α was set at $p < 0.05$ in both cases.

Fluorescence Lifetime Measurements. The fluorescence lifetime of AF555-TNB was measured using an ISS K2 frequency domain fluorometer as described previously.[30,31] Rhodamine B in water was used as a lifetime standard, which has a 1.7 ns lifetime (http://www.iss.com/resources/reference/data_tables/StandardsLEDsLaserDiodes.html). Excitation was obtained using a diode emitting modulated light at 518 nm (ISS); fluorescence emission was collected subsequent to a long-pass filter (540 LP, Omega Optical).

Experimental conditions were AF555-TNB (~10 nM) in solution or bound to purified $scFv_{TNT}$ (1 μM) and AF555-TNB (~2 nm after final wash) bound to isolated frustules (10^6/mL) isolated from native or transformed diatoms. All measurements were taken at 25 °C.

Analysis of Fluorescence Intensity Decay. The frequency domain data were analyzed by fitting the time-dependent decay $I(t)$ of fluorescence to a sum of exponentials using nonlinear least-squares, as previously described:[20,21]

DOI: 10.1021/acssynbio.5b00191
ACS Synth. Biol. 2016, 5, 193−199

$$I(t) = \sum_{i=1}^{n} \alpha_i e^{-t/\tau_i}$$

where α_i are the pre-exponential factors, τ_i are the decay times, and n is the number of exponential components required to describe the decay. The intensity decay law is obtained from the frequency response of amplitude-modulated light and is characterized by the frequency-dependent values of the phase and the extent of demodulation. The values are compared with the calculated values from an assumed decay law until a minimum of the squared deviation (χ_R^2) is obtained. After the measurement of the intensity decay, the mean lifetime was calculated:

$$\bar{\tau} = \sum_{i=1}^{n} \alpha_i \tau_i$$

Weighted residuals were calculated as the difference between measured and fit data divided by the error of individual measurements (0.2° or 0.004 for phase shift and modulated anisotropy, respectively).

■ ASSOCIATED CONTENT

Supporting Information

The Supporting Information is available free of charge on the ACS Publications website at DOI: 10.1021/acssynbio.5b00191.

Additional figures and data. (PDF)

Supporting movie. (AVI)

■ AUTHOR INFORMATION

Corresponding Author

*E-mail: g.roesijadi@pnnl.gov.

Notes

The authors declare no competing financial interest.

■ ACKNOWLEDGMENTS

Drs. Nils Kroger and Nicole Poulsen (CUBE Center for Molecular Bioengineering, Dresden, DE) provided clones for Sil3 and its $Sil3_{T8}$ derivative; Drs. Ellen Goldman and Igor Medintz (Naval Research Laboratory, Washington, D.C.) provided clones for scFvs and sdAbs, and assistance in preparing fluorescent TNT surrogate compounds, respectively. Drs. Li-Jung Kuo and Valerie Cullinan (Pacific Northwest National Laboratory) contributed to synthesis of AF555-TNB and statistical analysis, respectively. This research was supported by the Defense Threat Reduction Agency (G.R. and T.C.S.), the Office of Naval Research (G.R. and G.L.R.), and the Environmental Molecular Sciences Laboratory (EMSL) (G.R. and T.C.S). Part of the research was performed using EMSL, a national scientific user facility sponsored by the DOE's OBER and located at PNNL.

■ REFERENCES

(1) Round, F. E., Crawford, R. M., and Mann, D. G. (1990) *Diatoms: Biology and Morphology of the Genera*, Cambridge University Press, Cambridge, U.K.

(2) Patwardhan, S. V. (2011) Biomimetic and bioinspired silica: recent developments and applications. *Chem. Commun. 47*, 7567−7582.

(3) Kroger, N., and Brunner, E. (2014) Complex-shaped microbial biominerals for nanotechnology. *WIREs Nanomed. Nanobiotechnol. 6*, 615−627.

(4) Sheppard, V., Scheffel, A., Poulsen, N., and Kroger, N. (2012) Live diatom silica immobilization of multimeric and redox-active enzymes. *Appl. Environ. Microbiol. 78*, 211−218.

(5) Marshall, K. E., Robinson, E. W., Hengel, S. M., Pasa-Tolic, L., and Roesijadi, G. (2012) FRET Imaging of Diatoms Expressing a Biosilica-Localized Ribose Sensor. *PLoS One 7*, e33771.

(6) Delalat, B., Sheppard, V. C., Rasi Ghaemi, S., Rao, S., Prestidge, C. A., McPhee, G., Rogers, M.-L., Donoghue, J. F., Pillay, V., Johns, T. G., Kroger, N., and Voelcker, N. H. (2015) Targeted drug delivery using genetically engineered diatom biosilica. *Nat. Commun. 6*, 8791−8791.

(7) Poulsen, N., Scheffel, A., Sheppard, V. C., Chesley, P. M., and Kroger, N. (2013) Pentalysine Clusters Mediate Silica Targeting of Silaffins in *Thalassiosira pseudonana*. *J. Biol. Chem. 288*, 20100−20109.

(8) Scheffel, A., Poulsen, N., Shian, S., and Kroger, N. (2011) Nanopatterned protein microrings from a diatom that direct silica morphogenesis. *Proc. Natl. Acad. Sci. U. S. A. 108*, 3175−3180.

(9) Poulsen, N., Berne, C., Spain, J., and Kroger, N. (2007) Silica immobilization of an enzyme through genetic engineering of the diatom *Thalassiosira pseudonana*. *Angew. Chem., Int. Ed. 46*, 1843−1846.

(10) Cao, H. S., Xiong, Y. J., Wang, T., Chen, B. W., Squier, T. C., and Mayer, M. U. (2007) A red Cy3-based biarsenical fluorescent probe targeted to a complementary binding peptide. *J. Am. Chem. Soc. 129*, 8672.

(11) Fu, N., Xiong, Y., and Squier, T. C. (2013) Optimized Design and Synthesis of a Cell-Permeable Biarsenical Cyanine Probe for Imaging Tagged Cytosolic Bacterial Proteins. *Bioconjugate Chem. 24*, 251−259.

(12) Walper, S. A., Anderson, G. P., Lee, P. A. B., Glaven, R. H., Liu, J. L., Bernstein, R. D., Zabetakis, D., Johnson, L., Czarnecki, J. M., and Goldman, E. R. (2012) Rugged Single Domain Antibody Detection Elements for *Bacillus anthracis* Spores and Vegetative Cells. *PLoS One 7*, e32801.

(13) Liu, J. L., Zabetakis, D., Acevedo-Velez, G., Goldman, E. R., and Anderson, G. P. (2013) Comparison of an antibody and its recombinant derivative for the detection of the small molecule explosive 2,4,6-trinitrotoluene. *Anal. Chim. Acta 759*, 100−104.

(14) Poulsen, N., Chesley, P. M., and Kroger, N. (2006) Molecular genetic manipulation of the diatom *Thalassiosira pseudonana* (Bacillariophyceae). *J. Phycol. 42*, 1059−1065.

(15) Karas, B. J., Diner, R. E., Lefebvre, S. C., McQuaid, J., Phillips, A. P. R., Noddings, C. M., Brunson, J. K., Valas, R. E., Deerinck, T. J., Jablanovic, J., Gillard, J. T. F., Beeri, K., Ellisman, M. H., Glass, J. I., Hutchison, C. A., Smith, H. O., Venter, J. C., Allen, A. E., Dupont, C. L., and Weyman, P. D. (2015) Designer diatom episomes delivered by bacterial conjugation. *Nat. Commun. 6*, 6925.

(16) Dunn, K. W., Kamocka, M. M., and McDonald, J. H. (2011) A practical guide to evaluating colocalization in biological microscopy. *Am. J. Physiol.: Cell Physiol. 300*, C723−C742.

(17) Shimizu, K., Del Amo, Y., Brzezinski, M. A., Stucky, G. D., and Morse, D. E. (2001) A novel fluorescent silica tracer for biological silicification studies. *Chem. Biol. 8*, 1051−1060.

(18) Hildebrand, M., Frigeri, L. G., and Davis, A. K. (2007) Synchronized growth of *Thalassiosira pseudonana* (Bacillariophyceae) provides novel insights into cell-wall synthesis processes in relation to the cell cycle. *J. Phycol. 43*, 730−740.

(19) Tesson, B., and Hildebrand, M. (2013) Characterization and Localization of Insoluble Organic Matrices Associated with Diatom Cell Walls: Insight into Their Roles during Cell Wall Formation. *PLoS One 8*, e61675.

(20) Bevington, P. R. (1969) *Data Reduction and Error Analysis for the Physical Sciences*, McGraw-Hill, New York.

(21) Hunter, G. W., and Squier, T. C. (1998) Phospholipid acyl chain rotational dynamics are independent of headgroup structure in unilamellar vesicles containing binary mixtures of dioleoyl-phosphatidylcholine and dioleoyl-phosphatidylethanolamine. *Biochim. Biophys. Acta, Biomembr. 1415*, 63−76.

DOI: 10.1021/acssynbio.5b00191
ACS Synth. Biol. 2016, 5, 193−199

(22) Chen, H., Ahsan, S. S., Santiago-Berrios, M. E. B., Abruna, H. D., and Webb, W. W. (2010) Mechanisms of Quenching of Alexa Fluorophores by Natural Amino Acids. *J. Am. Chem. Soc. 132*, 7244−7245.
(23) Rusmini, F., Zhong, Z., and Feijen, J. (2007) Protein immobilization strategies for protein biochips. *Biomacromolecules 8*, 1775−1789.
(24) Hildebrand, M., York, E., Kelz, J. I., Davis, A. K., Frigeri, L. G., Allison, D. P., and Doktycz, M. J. (2006) Nanoscale control of silica morphology and three-dimensional structure during diatom cell wall formation. *J. Mater. Res. 21*, 2689−2698.
(25) Erickson, H. P. (2009) Size and Shape of Protein Molecules at the Nanometer Level Determined by Sedimentation, Gel Filtration, and Electron Microscopy. *Biol. Proced. Online 11*, 32−51.
(26) Hoffmann, C., Gaietta, G., Zurn, A., Adams, S. R., Terrillon, S., Ellisman, M. H., Tsien, R. Y., and Lohse, M. J. (2010) Fluorescent labeling of tetracysteine-tagged proteins in intact cells. *Nat. Protoc. 5*, 1666−1677.
(27) Goldman, E. R., Egge, A. L., Medintz, I. L., Lassman, M. E., and Anderson, G. P. (2005) Application of a homogenous assay for the detection of 2,4,6-trinitrotoluene to environmental water samples. *Sci. World J. 5*, 446−451.
(28) Schneider, C. A., Rasband, W. S., and Eliceiri, K. W. (2012) NIH Image to ImageJ: 25 years of image analysis. *Nat. Methods 9*, 671−675.
(29) Daniel, W. W. (1978) *Applied Nonparametric Statistics*, Houghton Mifflin Company.
(30) Gratton, E., and Limkeman, M. (1983) A continuously variable frequency cross-correlation phase fluorometer with picosecond resolution. *Biophys. J. 44*, 315−324.
(31) Lakowicz, J. R., and Maliwal, B. P. (1985) Construction and performance of a variable-frequency phase-modulation fluorometer. *Biophys. Chem. 21*, 61−78.

NOTE ADDED AFTER ASAP PUBLICATION

This paper was published ASAP on January 25, 2016, with incorrect panel descriptions in the caption of Figure 4. The corrected version was reposted on March 10, 2016.

DOI: 10.1021/acssynbio.5b00191
ACS Synth. Biol. 2016, 5, 193−199